ACS Photonics

pubs.acs.org/journal/apchd5

Article

Dynamically Tunable Asymmetric Transmission in PT-Symmetric Phase Gradient Metasurface

Jinal Tapar, Saurabh Kishen, and Naresh Kumar Emani*

Cite This: *ACS Photonics* 2021, 8, 3315−3322

Read Online

ACCESS | Metrics & More | Article Recommendations | Supporting Information

ABSTRACT: Active optical metasurfaces have attracted significant research attention in recent times. The conventional thermal and free-carrier induced index-tuning mechanisms have been widely explored to realize dynamic modulation of the optical properties. However, their modulation efficiency is limited by the intrinsic response of functional materials. The recent advances in the concept of PT (parity-time) symmetry and spatiotemporal modulation of permittivity have opened new avenues to realize dynamic tunability. In this work, we propose an all-dielectric PT-symmetric metasurface to tune the intensity and angular response of light through dynamic gain−loss modulation. Our approach shows tunable asymmetric transmission in a vertically stacked $Ga_{0.5}In_{0.5}P$ phased-array metasurface. The overall metasurface is optimized for operation at a wavelength of 655 nm (typical PL emission peak of $Ga_{0.5}In_{0.5}P$). The transmission is predominantly in the zeroth diffraction order ($\eta_0 \sim 0.80$, $\eta_1 \sim 0.18$) for loss side normal incidence, and an amplified transmission is observed in the first diffraction order ($\eta_0 \sim 0.04$, $\eta_1 \sim 0.79$) for gain side incidence. In addition to the asymmetric transmission for normal incidence, the proposed metasurface also exhibits asymmetric amplification in transmission for oblique incidence. An optimal arrangement of gain−loss resonators combined with tunable pumping (either optical or electrical) can pave the way toward on-chip reconfigurable nanophotonic devices.

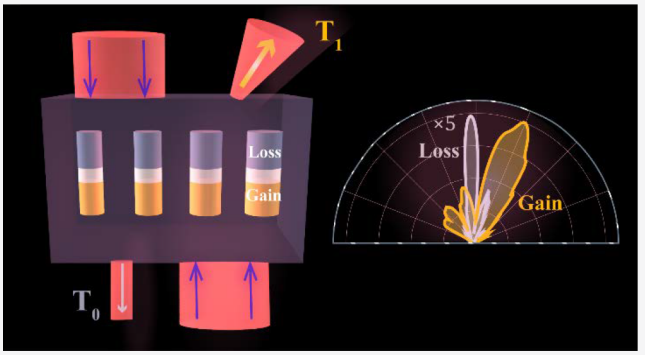

KEYWORDS: *PT (parity-time) symmetry, phase-gradient metasurface, asymmetric transmission, tunable all-dielectric metasurface, spectral singularity*

The ability to control the intrinsic properties of light (*viz.*, phase, intensity, wavevector, and polarization) using passive subwavelength structures has enabled the development of numerous beam-shaping photonic metasurfaces.[1,2] Beam shaping relies on engineering the phase accumulation as the wave propagates through the metasurface.[3,4] The desired phase profile for a passive metasurface is defined by the physical shape and arrangement of resonators, thus, fixing the geometry-induced scattering properties at the time of fabrication. The development of tunable active metasurfaces, which enable the dynamic control of light, has gained momentum in recent times.[5,6] This opens the possibility of realizing reconfigurable beam steering at optical wavelengths, with potential applications in optical switching, adaptive display technologies, and varifocal lenses, to name a few.[7,8] In this context, one of the long-standing challenges has been to develop practical and efficient techniques to arbitrarily mold the outgoing wavefront of an optical source or a localized nanoantenna. Dynamic tunability can be attained by a variety of methods, including but not limited to (i) index tuning of functional materials via external stimuli such as temperature, optical pumping, or electrical bias (like ITO, phase-change materials, liquid crystals, etc.),[9−12] (ii) modification of carrier concentrations by electrical or optical pumping in direct bandgap semiconductors and graphene,[13−16] (iii) manipulation of resonances by mechanical means,[17] for example, metasurface on a stretchable substrate,[18] and lately, spatiotemporal modulation of permittivity.[19−21] The modulation depth, speed, and power consumption are some of the important criteria for evaluating the efficacy of these techniques.[22] Despite tremendous progress, the dependence of these techniques on the intrinsic properties of the functional materials hinders large-scale optical integration. There is a need for further research to explore plausible ways for advancing dynamic tunability in compact nanophotonic devices.

The concept of parity-time (PT) symmetry[23,24] has generated new prospects for dynamic light control by allowing

Received: August 3, 2021
Published: November 8, 2021

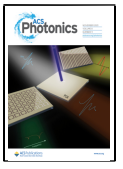

https://doi.org/10.1021/acsphotonics.1c01178
ACS Photonics 2021, 8, 3315−3322

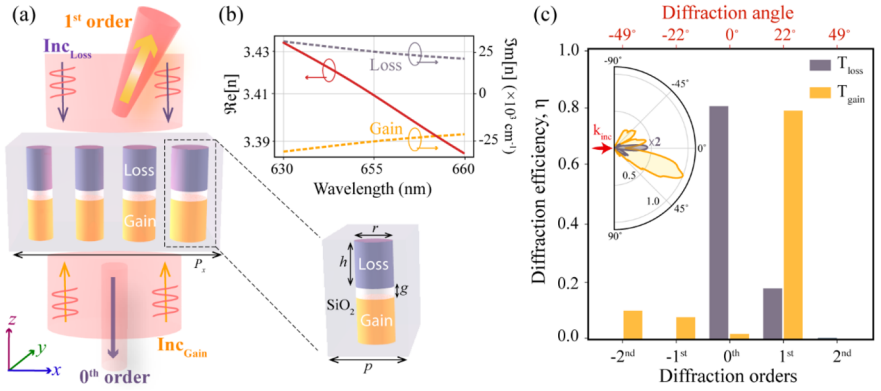

Figure 1. (a) Schematic illustration of the PT-symmetric GaInP metasurface with TM polarized plane wave light (E-field along the x-axis at normal incidence); gain−loss modulation is along the z-axis and it is parallel to the incident wave. The phase gradient is introduced along the x-axis with increasing radii of nanopillars. The height of the gain and loss nanodisks is h = 250 nm each. The coupling between the gain and loss GaInP nanodisks is determined by the gap thickness (g = 108 nm) of the SiO_2 layer, and the overall structure is embedded in SiO_2 to provide a symmetric environment. For top-side illumination (i.e., loss side), the transmission occurs primarily in the 0th order and is weakly amplified. In contrast, when illuminated from the bottom (gain side), an amplified transmission occurs predominantly in the 1st diffraction order. (b) The refractive index exhibits dispersion of the form $n(z, \lambda) = n^*(-z, \lambda)$, which satisfies the PT-symmetry condition. Note that the imaginary part of the index is expressed in terms of absorption/gain coefficient. (c) The relative diffraction efficiency ($\eta_m = T_m/T_{tot}$) and the far-field radiation pattern (inset) of transmitted power at λ = 655 nm. The radiation pattern is normalized with its maximum value, which occurs asymmetrically for loss and gain side incidences. The diffraction efficiency for loss side incidence is $\eta_0 \sim 0.8$, and the far-field transmission lobe is along the normal direction. For the gain side incidence, the diffraction efficiency is $\eta_1 \sim 0.79$, with the maximum power being refracted along an angle, $\theta \sim 22°$, corresponding to the 1st diffraction order. A 4-fold amplification is observed for gain side incidence compared to the loss side.

the modulation of the imaginary part of the refractive index. Broadly, PT symmetry implies that the system is invariant under both mirror-reflection (P-parity) and gain and loss reversal (T-time) operations.[25] The remarkable properties of PT-symmetric systems near exceptional points (EPs)[24,26] and spectral singularities (SS),[27,28] coupled with the flexibility to dynamically vary the amount of gain, has led to the demonstration of anisotropic scattering in a PT-symmetric plasmonic dimer,[29] preferential directionality in a PT-symmetric Janus cylinder,[30] unidirectional cloaking,[31] tunable degree of spatial coherence,[32] active polarization control,[33] and nonreciprocal directional amplification by temporal gain−loss modulation in a dielectric waveguide structure.[34] There is growing interest in extending the concept of PT-symmetry to higher-dimensional systems like photonic crystals and metasurfaces, which offer a broader design parameter space than the predominantly 1D or quasi-1D structures studied so far.[35−37] In this paper, we investigate the influence of the physical effects of PT-symmetry combined with a two-dimensional (2D) phase gradient metasurface on the transmission spectrum. We show that the proposed structure allows dynamic control of the angular scattering, amplitude, and efficiency of optical emission by modulating the amount of gain−loss in the system.

Numerical Modeling. The proposed structure is a two-dimensional metasurface, with each unit cell consisting of vertically stacked PT-symmetric $Ga_{0.5}In_{0.5}P$ nanopillars with varying radii, as schematically illustrated in Figure 1a. Here onward, we will address the material simply as GaInP. The primary block of this supercell is a square lattice with interpillar spacing p = 300 nm. The phase gradient is introduced along the x-direction with four-level discretization by choosing the nanopillars with radii 75, 85, 100, and 110 nm, making the supercell periodicity P_x = 1200 nm. This breaks the left−right symmetry of the metasurface. In the y-direction, the metasurface is subdiffractive with periodicity P_y = 300 nm. The gain−loss modulation is incorporated along the z-direction, *i.e.* longitudinal to the wave propagation direction, to realize PT symmetry.

The refractive index profile for the GaInP[38] meta-atom, with dispersion, in the wavelength range of ∼630−660 nm is shown in Figure 1b. The gain−loss modulation satisfies the complex refractive index condition of $n(-z, \lambda) = n^*(z, \lambda)$, thus, breaking the up−down symmetry. The geometric parameters of the metasurface are optimized to get maximum asymmetry at the wavelength of λ = 655 nm (typical photoluminescence (PL) peak of GaInP). We note that the proposed metasurface design can be scaled to other desired wavelengths, provided that a material capable of providing gain at the given wavelength is available and the geometric parameters are optimized accordingly. The proposed GaInP metasurface can be realized experimentally by choosing the loss resonator to have intrinsic doping (and hence low gain) and the gain resonator to have moderate p-doping (hence high gain;[39] see Supporting Information, S1, for experimental feasibility). The structure is studied numerically by carrying out full-wave three-dimensional (3D) simulations using Finite Element Method (COMSOL Multiphysics). The simulation domain consists of a rectangular supercell of the 2D array with periodic Bloch boundary conditions along the x and y directions. The stacked nanopillars representing the PT-symmetric GaInP resonators are excited using port boundary conditions at the top and bottom of the unit cell. The incident light is TM-polarized, with an electric field oriented along the x-axis. The scattered power in various diffraction orders supported by the lattice is computed by adding the required diffraction orders in both transmission and reflection ports.

Asymmetric Transmission for Normal Incidence. We first show that the transmission from the proposed metasurface is asymmetric for gain and loss side incidence; the asymmetry is manifested in both refraction angle and transmitted power. Despite asymmetric transmission, we note that the proposed structure is a reciprocal device as the materials considered are linear and time-independent, with a symmetric permittivity

https://doi.org/10.1021/acsphotonics.1c01178
ACS Photonics 2021, 8, 3315−3322

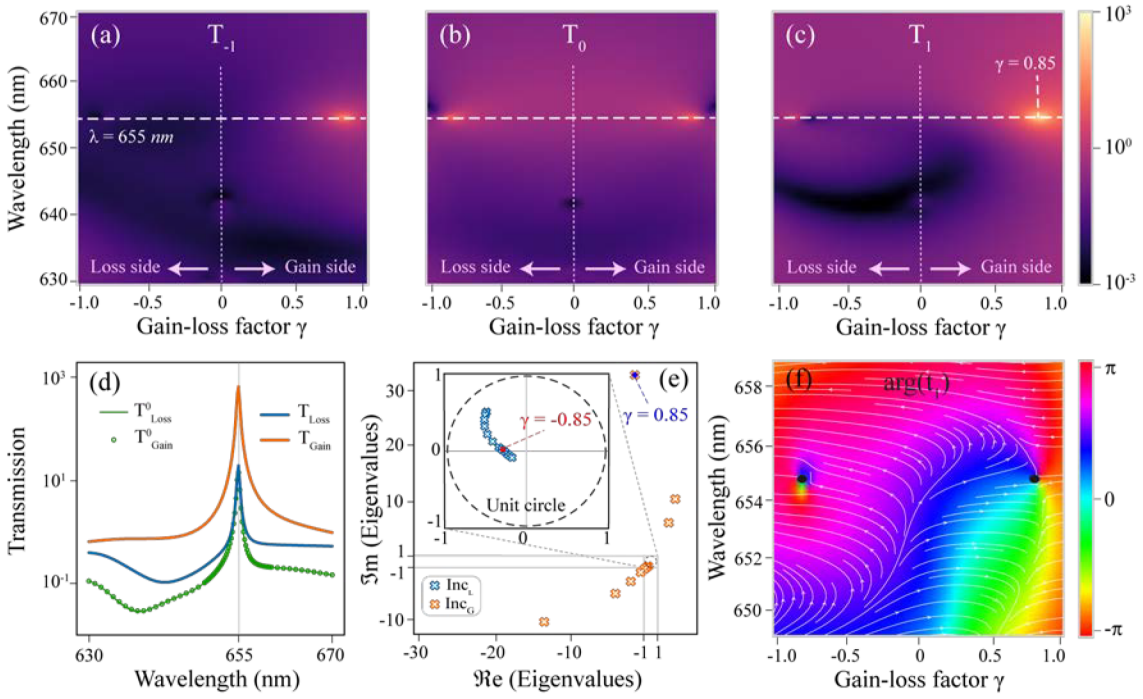

Figure 2. Transmission spectra as a function of gain−loss factor γ ($\gamma = 0$ represents a Hermitian system whereas $\gamma \neq 0$ represents a non-Hermitian system, with −ve and +ve values of γ corresponding to incidence from loss and gain side respectively). (a−c) The transmission is identical for illumination from both the loss and gain side incidence in the 0th order, while asymmetry is observed in −1st and 1st diffraction order for either side incidence. Extreme asymmetry is observed at $\gamma = 0.85$ and $\lambda = 655$ nm, corresponding to the occurrence of spectral singularity. (d) Transmission at SS shows a diverging peak for gain side incidence, which is ∼2 orders of magnitude larger than that for loss side incidence. Note that the 0th order transmission is identical. (e) Eigenvalues of the scattering matrix as a function of gain−loss factor γ. Two subsets of eigenvalues, one corresponding to loss side incidence shows subunitary evolution (lies inside the unit circle, as illustrated in the inset), while the other subset corresponding to gain side incidence far exceeds unit circle, implying amplification. This shows that the system is in the PT-symmetric phase for loss side incidence and the PT-broken phase for gain side incidence. (f) Phase plot for 1st order transmission coefficient. At $\gamma = 0.85$ and $\lambda = 655$ nm, phase singularity is evident with a topological charge of −1 (clockwise encirclement of 2π phase).

tensor.[40] Figure 1c shows the diffraction efficiency of the proposed metasurface for loss and gain side normal incidence. Here, with the optical gain being involved, we compute the relative diffraction efficiency by taking the power ratio in a given diffraction order (T_m) to the total transmitted power (T_{tot}), given by $\eta_m = T_m/T_{tot}$. The maximum diffraction efficiency for transmission is in the zeroth order for loss side incidence, corresponding to value $\eta_0 \sim 80\%$, while for gain side incidence, the maximum diffraction efficiency is observed in the + first diffraction order, $\eta_1 \sim 79\%$. The inset shows the far-field radiation pattern of the transmitted power. The transmission lobe is predominantly in the normal direction for loss side incidence, whereas for the gain side incidence, an amplified transmission lobe, is directed along $\theta = 22°$, corresponding to the first diffraction order.

Amplitude Control by Varying the Gain−Loss Factor. To demonstrate active tunability of transmission with optical pumping in the proposed metasurface, we analyzed (i) the strength of the direction-dependent amplification and (ii) the angular radiation pattern of the transmission lobe with dynamic control of gain and loss in the system. We define the non-Hermiticity factor, $\xi = \gamma \times \mathcal{J}m(n)$, where γ is the modulation parameter, also referred to as the gain−loss factor, and $\mathcal{J}m(n)$ is the magnitude of gain and loss coefficients for GaInP. A Hermitian system with no loss and gain is represented by $\gamma = 0$, whereas $\gamma \neq 0$ represents a non-Hermitian system; the value of $\gamma = 1$ indicates the maximum possible absorption and gain coefficients upon optical pumping (typical values shown in Figure 1b).

Figure 2a−c shows the transmission for normal incidence in different diffraction orders as a function of the wavelength and gain−loss factor (γ). With our notation, negative values of γ refer to incidence from the loss side of the metasurface, while positive γ corresponds to the gain side incidence. The transmission in the zeroth order, T_0, is identical for illumination from loss and gain side, that is, for either sign-parity of γ. In contrast, asymmetric power distribution can be observed in the −1st and 1st order. The highest asymmetry occurs at $|\gamma| = 0.85$, corresponding to the emergence of lasing spectral singularity (SS). In ref 41, Krasnok *et al.* have categorized different scattering anomalies based on zeros and poles of the scattering matrix (S-matrix) constructed using complex-valued scattering coefficients. The spectral singularity is categorized as one of the scattering anomalies wherein the scattering coefficients show a divergent behavior. The divergence of the total transmission (and reflection, not shown here) at $\lambda = 655$ nm is evident in Figure 2d. According to the literature, the divergent characteristics at SS are analogous to the unbounded scattering behavior at the lasing threshold.[42]

Nonetheless, there is a subtle distinction between conventional lasing behavior and the SS anomaly observed here at $|\gamma| = 0.85$. In a conventional laser, the light trapped inside a high-Q cavity experiences amplification when the net gain of the active material overcomes the cavity and material losses at the

https://doi.org/10.1021/acsphotonics.1c01178
ACS Photonics 2021, 8, 3315−3322

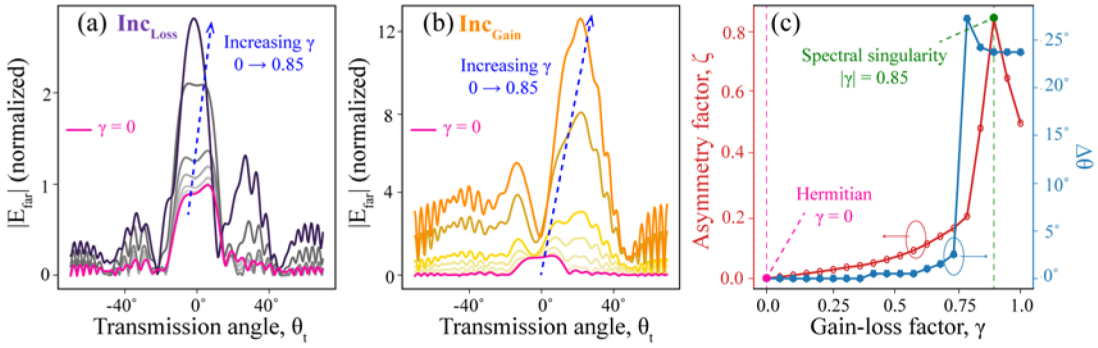

Figure 3. Far-field radiation pattern of transmission with increasing $\gamma \rightarrow 0$ to 0.85. (a) The dominant angular lobe for incidence from the loss side progresses along the normal direction, reaching ~3-fold amplification at SS, whereas (b) for gain side incidence, the dominant radiation lobe advances toward the 1st diffraction angle, attaining ~12-fold amplification. (Normalization is done with reference to the Hermitian case, $\gamma = 0$, highlighted in magenta color.) (c) Asymmetry factor ζ (left axis) and angular deviation $\Delta\theta$ (right axis) of transmission with varying gain−loss contrast. At $\gamma = 0.85$ (SS), the maximum asymmetry in transmission amplitude is ~0.9, and the angular asymmetry is ~24°.

lasing threshold. The overall losses in the system are predefined by the cavity design and material composition. Hence, with a further increment in gain above the lasing threshold, the light continues to amplify until the gain saturation is reached. Whereas in the case of SS, the light trapping dynamics for amplification are predominantly governed by the amount of loss and gain in the system. The phase acquired in both loss and gain materials facilitates building high-Q resonance. At the optimum phase condition, when the amplification perfectly balances the radiation losses, the outgoing scattered fields become divergent. In contrast to the conventional laser, an additional increment of gain or loss in the system perturbs the critical phase condition contributing to amplification, and hence, the divergence falls off. It should not be surprising as the similar counterintuitive pump-dependence of the laser has been experimentally demonstrated in PT-symmetric systems near an EP.[43,44] Similar works relating to the scattering anomalies' emergence and behavioral evolution with varying amounts of gain−loss in the photonic system could be found in refs 45 and 46. With this observation, we show that adding a large amount of gain to the system is not necessary. Rather, a careful design of the structure will lead to the occurrence of SS, even with lower gain values.

To get further insight into PT-dynamics in the proposed system, we plot the eigenvalues of a scattering (S) matrix for varying gain−loss contrast γ at wavelength $\lambda = 655$ nm, as shown in Figure 2e. It can be seen that there are two subsets of eigenvalues corresponding to incidence from the loss and gain side of the metasurface. A unit circle that signifies the unitarity of the S-matrix for a Hermitian system is shown in the dashed line. The eigenvalues of a system deviate from the unit circle whenever the PT-symmetric system is in broken-phase.[25] A branch of eigenvalues corresponding to incidence from loss and gain sides lie inside and outside the unit circle, respectively, as illustrated in the inset of Figure 2e. At the spectral singularity, the eigenvalue corresponding to gain side incidence at $\gamma = 0.85$ far exceeds the unit circle, implying strong amplification. The observed asymmetry in the transmission is a direct consequence of the emergence of different states of the PT-phase for either side of incidence: PT-unbroken phase for loss side incidence and broken PT-phase for gain side incidence. Figure 2f shows the phase response in the first-order transmission. The scattering phase is undefined at $\gamma = 0.85$ and $\lambda = 655$ nm in the given parameter space, resulting in a phase singularity. The integral phase (modulo 2π) encircling the phase singularity is defined as the topological charge q, and the direction of the encirclement determines its sign. As per the convention, counterclockwise encirclement is termed as positive charge and vice versa. The phase singularity at $\gamma = 0.85$ has a topological charge $q = -1$. The ability to obtain lasing with the associated phase singularity will find applications in generating arbitrarily oriented spatiotemporal vortex beams, as proposed in ref 47.

Directivity Control by Varying the Gain−Loss Factor. To analyze the directional behavior of transmission as a function of the modulation parameter, we plotted the normalized angular far-field radiation pattern for varying γ, as shown in Figure 3a,b. For reference, we have plotted the radiation pattern for the Hermitian case ($\gamma = 0$) in magenta. For loss side incidence (Figure 3a), the transmission lobe becomes stronger and narrower along the normal direction as the system is tuned away from the Hermitian regime and attains a moderate amplification (~3-fold) relative to the Hermitian case. While for gain side illumination (Figure 3b), the dominant radiation lobe moves toward angle $\theta \sim 22°$, corresponding to the first diffraction order with increasing non-Hermiticity and attains the peak amplification ~12-fold at $\gamma = 0.85$. The overall variation in the amplitude and angular spectrum of transmission with varying gain−loss factor is summarized in Figure 3c. We define the asymmetry factor $\zeta = (T_{gl} - T_{lg})/(T_{gl} + T_{lg})$, where T_{gl} and T_{lg} represent transmission when light propagates from gain-to-loss and loss-to-gain sides, respectively. The asymmetry factor $\zeta = 0$ for the Hermitian case as the up−down symmetry is preserved in the absence of optical loss and gain. With increasing non-Hermiticity ($\gamma \rightarrow 0$ to 1), the asymmetry increases gradually, with a sharp rise at $\gamma = 0.85$, wherein the SS emerges. The maximum difference between the two opposite-side transmissions is around ~90% for $\lambda = 655$ nm. Similarly, we calculated the difference in the angular direction of the dominant transmission lobe as a function of γ, given by $\Delta\theta = |\theta_{gl}| - |\theta_{lg}|$, plotted on the right-side axis in Figure 3c. At $\gamma = 0.85$, corresponding to the maximum asymmetry in the transmission amplitude, the emission lobes differ spatially by an angle $\Delta\theta \sim 24°$. Here, the pump intensity controls the PT-symmetry dynamics and is integral to breaking and restoring up−down symmetry. Thus, the transmission properties of the proposed metasurface can be continuously tuned by varying the strength of gain−loss in the system, demonstrating

https://doi.org/10.1021/acsphotonics.1c01178
ACS Photonics 2021, 8, 3315−3322

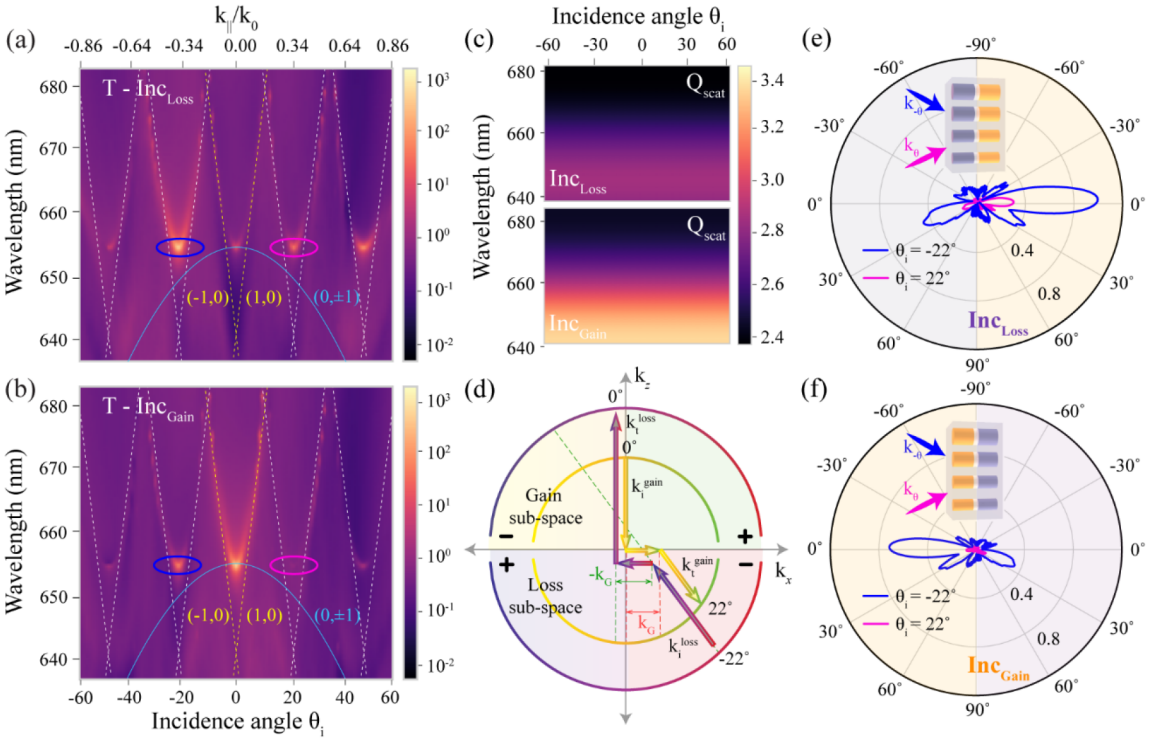

Figure 4. Transmission spectra for oblique incidence from (a) loss and (b) gain side of the metasurface. In addition to the asymmetric transmission for the loss and gain side incidences, there is an asymmetry with respect to $+\theta_i$ and $-\theta_i$ angles of incidence. Linear and parabolic dispersion corresponding to (±1, 0) and (0, ±1) RAs, respectively for p = 300 nm, are highlighted with dotted yellow lines and solid blue curves. The (±1, 0) linear dispersion is repeated along the angles corresponding to ±1st and ±2nd diffraction orders for P_x = 1200 nm. (c) Mie scattering efficiency of single PT-symmetric nanocylinder (r = 85 nm) shows a broader peak with asymmetric efficiencies for incidence from loss and gain sides. Notably, the dispersion is flat, showing no dependence on the parallel momentum, $k_{\|}$. Amplified spectral peaks (bright spots) appear at the locations of Mie-SLRs, corresponding to the coupling of individual PT-symmetric resonators through in-plane diffraction orders (RAs). (d) By virtue of reciprocity, the transmission for incidence at $\theta_i = -22°$ from the loss side is largely amplified in accordance to the observed amplification in the 1st order diffraction channel ($\theta_t = -22°$) for normal incidence from the gain side. The radiation pattern for incidence from angles $|\theta_i| = 22°$ from (e) loss and (f) side of the metasurface. The radiation patterns, in either case, are similar but show asymmetric amplification with respect to +ve and −ve angle. Transmission from the loss side experiences relatively more amplification compared to the gain side. The asymmetric transmission from the loss and gain sides is due to the breaking of up−down and left−right symmetries for angular incidence, providing different interaction paths through the resonant and nonresonant loss and gain nanoantennas.

direction-sensitive amplification and a tunable radiation pattern strongly dependent on the pump intensity.

Asymmetric Transmission for Oblique Incidence. In addition to the asymmetric transmission for normal incidence from gain and loss sides, the proposed metasurface exhibits broken symmetry for waves incident from $+\theta_i$ and $-\theta_i$ angles, respectively. Figure 4a,b shows the transmission spectra for loss and gain side incidence with the angle of incidence swept from $\theta_i \rightarrow -60°$ to 60° or equivalently, the in-plane momentum corresponding to $k_{\|}^{i} = k_0 \sin(\theta_i)$, where $k_0 = 2\pi/\lambda$. It is well-known that the collective diffraction in the periodic arrangement of plasmonic scatterers leads to spectrally narrow surface modes called surface lattice resonances (SLRs).[48] A similar phenomenon is observed in dielectric metasurfaces formed by Mie scatterers in periodic arrangements, termed Mie-SLRs.[48] The superposition of sharp lattice resonances arising through in-plane diffraction orders (also called Rayleigh anomalies RAs),[49] with the broad localized Mie resonances of the individual scatterers, result in the overall enhancement of light scattering while imparting directivity.[50,51] The RA condition for radiative modes in a square lattice with pitch p = 300 nm is given by $n_{SiO_2}k_0 = \sqrt{(k_x + m_1G)^2 + (k_y + m_2G)^2}$, where $G = 2\pi/p$ is the lattice momentum, m_1 and m_2 are the integers corresponding to Bragg diffraction order along x and y directions, respectively. Figure 4c shows spectra of scattering efficiency Q_{scat} of individual PT-symmetric nanocylinders (r = 85 nm) for varying oblique incidence from the loss and gain side of the nanocylinder. The dispersionless behavior of the Q_{scat} band with respect to in-plane momentum $k_{\|}$ is due to the localized nature of Mie resonances of individual nanocylinders. We note that the scattering efficiency is asymmetric for incidence from the loss and gain sides. The enhanced transmission, seen as bright spots in Figure 4a,b, arises from the hybridization of multipolar Mie resonances with RAs. The dispersion of amplified transmission follows the RA condition; the linear dispersion, highlighted with dotted lines in Figure 4a,b, corresponds to (±1, 0) diffraction orders in the plane of incidence (x−z). In contrast, parabolic dispersion, highlighted with solid blue curves, corresponds to the (0, ±1) order, perpendicular to the incidence plane (y−z). Indeed, the excellent correspondence of the dispersion of transmission peaks along the linear RA condition confirms the role of strong diffractive coupling in enhancing the light emission from the metasurface.

The maximum amplification of transmitted light is observed for normal incidence from the gain side (brightest spot in

https://doi.org/10.1021/acsphotonics.1c01178
ACS Photonics 2021, 8, 3315−3322

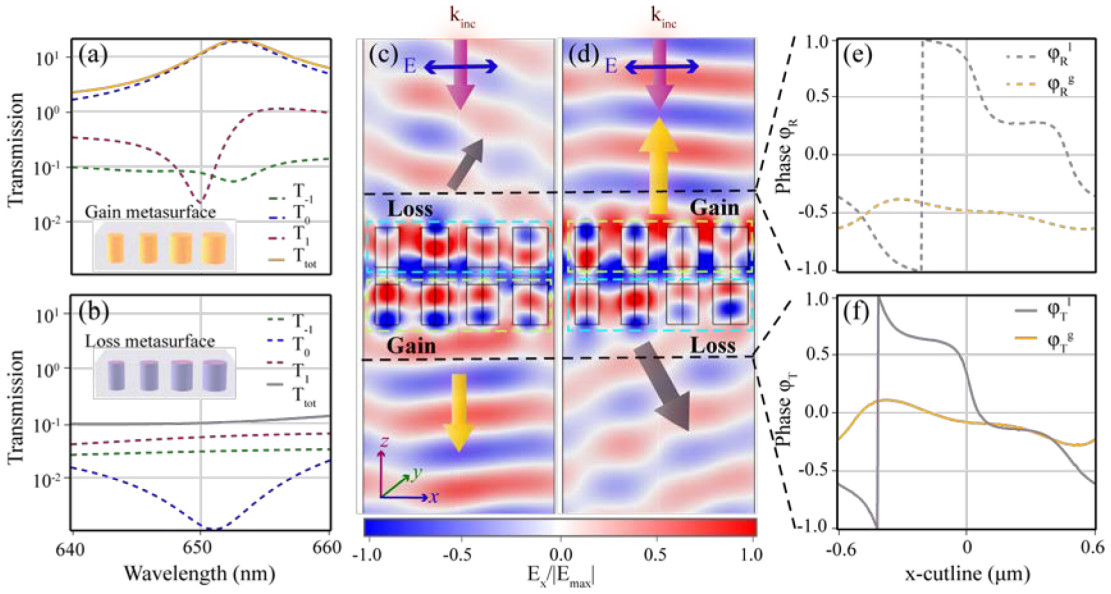

Figure 5. Transmission for a phase gradient metasurface consisting of (a) "only gain" nanodisks (h = 250 nm) show a moderately amplified peak in the 0th order, and that of (b) "only loss" nanodisks (h = 250 nm) show attenuation with the power predominantly in the 1st diffraction order. Transverse electric field profile E_x for normal incidence from the (c) loss and (d) gain side of the metasurface. The power emission from the gain-side layer of metasurface (either transmission or reflection, depicted by bold yellow arrows) is along the normal direction, manifesting the slab-like nature due to strong near-field coupling. At the same time, the wavefront (bold gray arrows) tilts when exiting from the loss-side layer of the metasurface, illustrating the phase gradient characteristic. The phase profile across the cut lines (black dashed) on the (e) reflection and (f) transmission is almost flat on the gain side, while it shows 2π wrapping on the loss-side layer.

Figure 4b) and also for oblique incidence at $\theta_i = -22°$ from the loss side (brightest spot in Figure 4a). We explain this observation using the principle of reciprocity, schematically illustrated in Figure 4d. The resultant momentum of transmitted light with gain side incidence can be given as $k_t^{gain} = k_i^{gain} + k_G$, where $k_G = 2\pi/P_x$ is the additional momentum imparted by phase gradient (details discussed in the subsequent section). By virtue of reciprocity, if we traverse back along $\theta_i = 22°$ from the loss side, the resultant momentum relation follows as $k_t^{loss} = k_i^{loss} - k_G$, making the light transmit again in first diffraction order, making $\theta_t = 0°$ on the gain side. (Following the sign convention with respect to incidence from the $\pm z$ axis, $\theta_i = 22°$ from the loss side effectively translates to $\theta_i = -22°$). This further confirms that the proposed system is a reciprocal device, despite the asymmetric response of the transmission.

We plot the far-field radiation pattern for the angle of incidence corresponding to −1st and 1st diffraction angle, $|\theta_i| = 22°$ from loss and gain side incidence, as shown in Figure 4e and f, respectively. Although the radiation patterns for positive and negative angles of incidence in each figure are similar, there is an asymmetric amplification in the far-field pattern. In contrast to normal incidence, the transmission for oblique incidence from the loss side experiences relatively more amplification than the gain side. Up−down symmetry breaking associated with PT-symmetric potential excites a different set of electric and magnetic multipoles depending on the illumination direction; the broken left−right symmetry due to phase gradient provides a different interaction path for light. The combined effect of broken up−down and left−right symmetries on the wave propagation in the respective directions is integral to realizing asymmetric response. Thus, interesting directional scattering patterns or even complete suppression of radiation from one side of angular incidence can be realized by tailoring the interaction path of light through resonant/nonresonant gain and loss nanoantennas.

DISCUSSION

For a phase gradient metasurface, the in-plane momentum of incoming ($k_\parallel^i = k_0 \sin(\theta_i)$) and outgoing ($k_\parallel^t = k_0 \sin(\theta_t)$) plane waves are related through generalized Snell's law, given by $k_\parallel^t = k_\parallel^i + k_G$, where $k_G = 2\pi/P_x = \nabla\varphi$ is an additional momentum imparted by the geometric phase gradient.[3] To better understand the observed emission properties of the metasurface, we present a simple model by separating the bilayer metasurface into gain and loss sublayers. We show here that for loss (gain) side incidence, the gain (loss) resonators predominantly decide the amplitude and direction of propagation of the transmitted wave. The proposed PT-symmetric stacked metasurface largely inherits the individual amplitude and phase response of its constituent sublayers, that is, the "only gain" and "only loss" metasurface.

We first analyze the transmission spectra for a gradient metasurface encompassing only gain and loss nanodisks, as shown in Figure 5a and b, respectively. The light transmission from "only gain" metasurface shows weak amplification with a peak around the wavelength λ = 654 nm and almost all the power being emitted in zeroth order. On the other hand, "only loss" metasurface shows significant attenuation in transmission ($T_{tot} \sim 0.1$), with most of the power being distributed in the 1st order. To understand the phenomenon of asymmetric emission and the role of these individual responses, we consider the electric field profile oriented along the x-direction (E_x), as the light propagates through the metasurface for loss and gain side incidence in Figure 5c and d, respectively. The electric field, E_x, is normalized with its maximum value for the respective sides of incidence. There are important observations to be made for light emission from either side of the

https://doi.org/10.1021/acsphotonics.1c01178
ACS Photonics 2021, 8, 3315−3322

metasurface: (i) The electric field, while exiting from the gain side of metasurface (either transmission or reflection), does not exhibit any significant phase gradient, that is, $\nabla\varphi \cong 0$. The four constituent nanoantennas of the supercell are strongly coupled in the near-field regime due to field amplification imparted by the gain media. This strong coupling gives the geometrically gradient supercell a unified slab-like behavior. The resultant in-plane momentum equates to $k_{\|}^{t} = k_{\|}^{i}$ as $k_G = 0$, directing the light as per Snell's law. (ii) The electric field exiting from the loss side of the metasurface shows a tilted field profile. Unlike the case of the gain-side metasurface, the four constituent nanoantennas on the loss side of the metasurface retain the lateral phase gradient response introduced by varying sizes of nanodisks. The resultant phase wrapping of $\nabla\varphi \cong 2\pi$ channels light into the desired angle, governed by the equation, $k_{\|}^{t} = k_{\|}^{i} + k_G$.

The accumulated phase of light emitted toward the reflection and transmission sides of the metasurface is plotted in Figure 5e,f. The phases are calculated along the cut lines across the transverse E-field plot shown in Figure 5c,d. The phase profile across the gain-side (yellow color lines) depicts a minimal phase gradient, while the phase along the loss-side (gray color lines) shows a 2π phase wrap in both the transmission and the reflection directions. This further reinforces our simple model and explains asymmetric light propagation for loss and gain side illumination.

CONCLUSION

In conclusion, we demonstrated a PT-symmetric phase-gradient metasurface that offers new possibilities for realizing dynamic control of light without relying on functional materials. We showed extreme asymmetry in transmission amplitude as well as far-field radiation pattern for normal and oblique incidence from either side of the metasurface. The maximum asymmetry is observed at a non-Hermiticity value of $\gamma = 0.85$, corresponding to the emergence of spectral singularity. As a proof of concept, we demonstrated dynamic beam steering with direction-dependent amplitude via gain–loss modulation. The asymmetry in emission is strongly dependent on the pump intensity and opens up the possibility of dynamically and reversibly tuning the optical emission properties of the metasurface. We note that the optical gain needed is practical ($\sim 10^4$ cm^{-1}) for experimental realization. Finally, we discussed the mechanism behind asymmetric amplification and angular emission spectrum by analyzing the individual transmission response of loss and gain sublayers of the metasurface. The key asset is the direction-dependent near-field coupling that imparts either a flat or a 2π phase profile. The prospect of dynamic control of the phase shift using external stimuli can lead to various breakthrough technological outcomes like beam steering, varifocal lenses, vortex beam generators, and nonreciprocal amplifiers/attenuators.

ASSOCIATED CONTENT

Supporting Information

The Supporting Information is available free of charge at https://pubs.acs.org/doi/10.1021/acsphotonics.1c01178.

Experimental feasibility of controlling the gain and loss in the structure by employing the variable gain quasi PT-symmetric metasurface (PDF)

AUTHOR INFORMATION

Corresponding Author

Naresh Kumar Emani − *Department of Electrical Engineering, Indian Institute of Technology, Hyderabad 502285, India;* orcid.org/0000-0002-0488-921X; Email: naresh@ee.iith.ac.in

Authors

Jinal Tapar − *Department of Electrical Engineering, Indian Institute of Technology, Hyderabad 502285, India*

Saurabh Kishen − *Department of Electrical Engineering, Indian Institute of Technology, Hyderabad 502285, India*

Complete contact information is available at: https://pubs.acs.org/10.1021/acsphotonics.1c01178

Funding

Science and Engineering Research Board (ECR/2018/002452, SB/S2/RJN-007/2017); Ministry of Education (STARS/APR2019/NS/774).

Notes

The authors declare no competing financial interest.

ACKNOWLEDGMENTS

J.T. and S.K. acknowledge the Ministry of Education (MOE), Government of India, for the research fellowship to undertake their Ph.D. studies.

REFERENCES

(1) Chen, H.-T.; Taylor, A. J.; Yu, N. A review of metasurfaces: physics and applications. *Rep. Prog. Phys.* **2016**, *79* (7), 076401.

(2) Genevet, P.; Capasso, F.; Aieta, F.; Khorasaninejad, M.; Devlin, R. Recent advances in planar optics: from plasmonic to dielectric metasurfaces. *Optica* **2017**, *4* (1), 139–152.

(3) Yu, N.; Genevet, P.; Kats, M. A.; Aieta, F.; Tetienne, J.-P.; Capasso, F.; Gaburro, Z. Light propagation with phase discontinuities: generalized laws of reflection and refraction. *Science* **2011**, *334* (6054), 333–337.

(4) Khorasaninejad, M.; Chen, W. T.; Devlin, R. C.; Oh, J.; Zhu, A. Y.; Capasso, F. Metalenses at visible wavelengths: Diffraction-limited focusing and subwavelength resolution imaging. *Science* **2016**, *352* (6290), 1190–1194.

(5) Hail, C. U.; Michel, A. K. U.; Poulikakos, D.; Eghlidi, H. Optical metasurfaces: evolving from passive to adaptive. *Adv. Opt. Mater.* **2019**, *7* (14), 1801786.

(6) Shalaginov, M. Y.; Campbell, S. D.; An, S.; Zhang, Y.; Ríos, C.; Whiting, E. B.; Wu, Y.; Kang, L.; Zheng, B.; Fowler, C.; Zhang, H.; Werner, D. H.; Hu, J.; Gu, T. Design for quality: reconfigurable flat optics based on active metasurfaces. *Nanophotonics* **2020**, *9* (11), 3505–3534.

(7) Berto, P.; Philippet, L.; Osmond, J.; Liu, C. F.; Afridi, A.; Marques, M. M.; Agudo, B. M.; Tessier, G.; Quidant, R. Tunable and free-form planar optics. *Nat. Photonics* **2019**, *13* (9), 649–656.

(8) Klopfer, E.; Lawrence, M.; Barton, D. R., III; Dixon, J.; Dionne, J. A. Dynamic focusing with high-quality-factor metalenses. *Nano Lett.* **2020**, *20* (7), 5127–5132.

(9) Huang, Y.-W.; Lee, H. W. H.; Sokhoyan, R.; Pala, R. A.; Thyagarajan, K.; Han, S.; Tsai, D. P.; Atwater, H. A. Gate-tunable conducting oxide metasurfaces. *Nano Lett.* **2016**, *16* (9), 5319–5325.

(10) Zou, C.; Amaya, C.; Fasold, S.; Muravsky, A. A.; Murauski, A. A.; Pertsch, T.; Staude, I. Multiresponsive Dielectric Metasurfaces. *ACS Photonics* **2021**, *8* (6), 1775–1783.

(11) Abdollahramezani, S.; Hemmatyar, O.; Taghinejad, H.; Krasnok, A.; Kiarashinejad, Y.; Zandehshahvar, M.; Alù, A.; Adibi, A. Tunable nanophotonics enabled by chalcogenide phase-change materials. *Nanophotonics* **2020**, *9* (5), 1189–1241.

(12) Wang, Y.; Landreman, P.; Schoen, D.; Okabe, K.; Marshall, A.; Celano, U.; Wong, H.-S. P.; Park, J.; Brongersma, M. L. Electrical tuning of phase-change antennas and metasurfaces. *Nat. Nanotechnol.* **2021**, *16*, 667−672.
(13) Iyer, P. P.; Pendharkar, M.; Palmstrøm, C. J.; Schuller, J. A. III−V heterojunction platform for electrically reconfigurable dielectric metasurfaces. *ACS Photonics* **2019**, *6* (6), 1345−1350.
(14) Emani, N. K.; Chung, T.-F.; Ni, X.; Kildishev, A. V.; Chen, Y. P.; Boltasseva, A. Electrically tunable damping of plasmonic resonances with graphene. *Nano Lett.* **2012**, *12* (10), 5202−5206.
(15) Shcherbakov, M. R.; Liu, S.; Zubyuk, V. V.; Vaskin, A.; Vabishchevich, P. P.; Keeler, G.; Pertsch, T.; Dolgova, T. V.; Staude, I.; Brener, I.; Fedyanin, A. A. Ultrafast all-optical tuning of direct-gap semiconductor metasurfaces. *Nat. Commun.* **2017**, *8* (1), 17.
(16) Wu, P. C.; Pala, R. A.; Shirmanesh, G. K.; Cheng, W.-H.; Sokhoyan, R.; Grajower, M.; Alam, M. Z.; Lee, D.; Atwater, H. A. Dynamic beam steering with all-dielectric electro-optic III−V multiple-quantum-well metasurfaces. *Nat. Commun.* **2019**, *10* (1), 1−9.
(17) Arbabi, E.; Arbabi, A.; Kamali, S. M.; Horie, Y.; Faraji-Dana, M.; Faraon, A. MEMS-tunable dielectric metasurface lens. *Nat. Commun.* **2018**, *9* (1), 1−9.
(18) Ee, H.-S.; Agarwal, R. Tunable metasurface and flat optical zoom lens on a stretchable substrate. *Nano Lett.* **2016**, *16* (4), 2818−2823.
(19) Caloz, C.; Deck-Léger, Z.-L. Spacetime metamaterials—part i: general concepts. *IEEE Trans. Antennas Propag.* **2020**, *68* (3), 1569−1582.
(20) Shaltout, A. M.; Shalaev, V. M.; Brongersma, M. L. Spatiotemporal light control with active metasurfaces. *Science* **2019**, *364* (6441), na.
(21) Caloz, C.; Deck-Léger, Z.-L. Spacetime metamaterials—Part II: Theory and applications. *IEEE Trans. Antennas Propag.* **2020**, *68* (3), 1583−1598.
(22) Taghinejad, M.; Cai, W. All-optical control of light in micro- and nanophotonics. *ACS Photonics* **2019**, *6* (5), 1082−1093.
(23) Longhi, S. Parity-time symmetry meets photonics: A new twist in non-Hermitian optics. *EPL-Europhys. Lett.* **2017**, *120* (6), 64001.
(24) Özdemir, Ş.; Rotter, S.; Nori, F.; Yang, L. Parity−time symmetry and exceptional points in photonics. *Nat. Mater.* **2019**, *18* (8), 783−798.
(25) Chong, Y.; Ge, L.; Stone, A. D. P t-symmetry breaking and laser-absorber modes in optical scattering systems. *Phys. Rev. Lett.* **2011**, *106* (9), 093902.
(26) Miri, M.-A.; Alù, A. Exceptional points in optics and photonics. *Science* **2019**, *363* (6422), eaar7709.
(27) Mostafazadeh, A. Spectral singularities of complex scattering potentials and infinite reflection and transmission coefficients at real energies. *Phys. Rev. Lett.* **2009**, *102* (22), 220402.
(28) Ramezani, H.; Li, H.-K.; Wang, Y.; Zhang, X. Unidirectional spectral singularities. *Phys. Rev. Lett.* **2014**, *113* (26), 263905.
(29) Manjavacas, A. Anisotropic optical response of nanostructures with balanced gain and loss. *ACS Photonics* **2016**, *3* (7), 1301−1307.
(30) Miri, M.-A.; Eftekhar, M. A.; Facao, M.; Abouraddy, A. F.; Bakry, A.; Razvi, M. A.; Alshahrie, A.; Alù, A.; Christodoulides, D. N. Scattering properties of PT-symmetric objects. *J. Opt.* **2016**, *18* (7), 075104.
(31) Sounas, D. L.; Fleury, R.; Alù, A. Unidirectional cloaking based on metasurfaces with balanced loss and gain. *Phys. Rev. Appl.* **2015**, *4* (1), 014005.
(32) Pires, D.; Litchinitser, N.; Brandão, P. Scattering of partially coherent vortex beams by a $\mathcal {PT} $-symmetric dipole. *Opt. Express* **2021**, *29* (10), 15576−15586.
(33) Baum, B.; Lawrence, M.; Barton, D., III; Dionne, J.; Alaeian, H. Active polarization control with a parity-time-symmetric plasmonic resonator. *Phys. Rev. B: Condens. Matter Mater. Phys.* **2018**, *98* (16), 165418.
(34) Song, A. Y.; Shi, Y.; Lin, Q.; Fan, S. Direction-dependent parity-time phase transition and nonreciprocal amplification with dynamic gain-loss modulation. *Phys. Rev. A: At., Mol., Opt. Phys.* **2019**, *99* (1), 013824.
(35) Zhen, B.; Hsu, C. W.; Igarashi, Y.; Lu, L.; Kaminer, I.; Pick, A.; Chua, S.-L.; Joannopoulos, J. D.; Soljačić, M. Spawning rings of exceptional points out of Dirac cones. *Nature* **2015**, *525* (7569), 354−358.
(36) Bandres, M. A.; Wittek, S.; Harari, G.; Parto, M.; Ren, J.; Segev, M.; Christodoulides, D. N.; Khajavikhan, M. Topological insulator laser: Experiments. *Science* **2018**, *359* (6381), na.
(37) Tapar, J.; Kishen, S.; Emani, N. K. Spectral singularities and asymmetric light scattering in PT-symmetric 2D nanoantenna arrays. *Opt. Lett.* **2020**, *45* (18), 5185−5188.
(38) Schubert, M.; Gottschalch, V.; Herzinger, C. M.; Yao, H.; Snyder, P. G.; Woollam, J. A. Optical constants of Ga x In1− x P lattice matched to GaAs. *J. Appl. Phys.* **1995**, *77* (7), 3416−3419.
(39) Tapar, J.; Kishen, S.; Prashant, K.; Nayak, K.; Emani, N. K. Enhancement of the optical gain in GaAs nanocylinders for nanophotonic applications. *J. Appl. Phys.* **2020**, *127* (15), 153102.
(40) Jalas, D.; Petrov, A.; Eich, M.; Freude, W.; Fan, S.; Yu, Z.; Baets, R.; Popovic, M.; Melloni, A.; Joannopoulos, J. D.; Vanwolleghem, M.; Doerr, C. R.; Renner, H. What is - and what is not - an optical isolator. *Nat. Photonics* **2013**, *7* (8), 579−582.
(41) Krasnok, A.; Baranov, D.; Li, H.; Miri, M.-A.; Monticone, F.; Alú, A. Anomalies in light scattering. *Adv. Opt. Photonics* **2019**, *11* (4), 892−951.
(42) Mostafazadeh, A. Optical spectral singularities as threshold resonances. *Phys. Rev. A: At., Mol., Opt. Phys.* **2011**, *83* (4), 045801.
(43) Brandstetter, M.; Liertzer, M.; Deutsch, C.; Klang, P.; Schöberl, J.; Türeci, H. E.; Strasser, G.; Unterrainer, K.; Rotter, S. Reversing the pump dependence of a laser at an exceptional point. *Nat. Commun.* **2014**, *5* (1), 1−7.
(44) Peng, B.; Özdemir, Ş.; Rotter, S.; Yilmaz, H.; Liertzer, M.; Monifi, F.; Bender, C.; Nori, F.; Yang, L. Loss-induced suppression and revival of lasing. *Science* **2014**, *346* (6207), 328−332.
(45) Kolkowski, R.; Koenderink, A. F. Gain-induced scattering anomalies of diffractive metasurfaces. *Nanophotonics* **2020**, *9* (14), 4273−4285.
(46) Nechepurenko, I.; Baranov, D.; Dorofeenko, A. Lasing induced by resonant absorption. *Opt. Express* **2015**, *23* (16), 20394−20401.
(47) Wang, H.; Guo, C.; Jin, W.; Song, A. Y.; Fan, S. Engineering arbitrarily oriented spatiotemporal optical vortices using transmission nodal lines. *Optica* **2021**, *8* (7), 966−971.
(48) Kravets, V. G.; Kabashin, A. V.; Barnes, W. L.; Grigorenko, A. N. Plasmonic Surface Lattice Resonances: A Review of Properties and Applications. *Chem. Rev.* **2018**, *118* (12), 5912−5951.
(49) Harvey, J. E.; Pfisterer, R. N. Understanding diffraction grating behavior: including conical diffraction and Rayleigh anomalies from transmission gratings. *Opt. Eng.* **2019**, *58* (8), 087105.
(50) Castellanos, G. W.; Bai, P.; Rivas, J. G. Lattice resonances in dielectric metasurfaces. *J. Appl. Phys.* **2019**, *125* (21), 213105.
(51) Vaskin, A.; Kolkowski, R.; Koenderink, A. F.; Staude, I. Light-emitting metasurfaces. *Nanophotonics* **2019**, *8* (7), 1151−1198.

https://doi.org/10.1021/acsphotonics.1c01178
ACS Photonics 2021, 8, 3315−3322